High-Temperature Scanning Tunneling Microscopy Study of the Ordering Transition of an Amorphous Carbon Layer into Graphene on Ruthenium(0001)

Sebastian Günther,[†] Sebastian Dänhardt,[‡] Martin Ehrensperger,[‡] Patrick Zeller,[‡] Stefan Schmitt,[§] and Joost Wintterlin[‡,⊥,*]

[†]Chemie Department, Technische Universität München, Lichtenbergstraße 4, D-85748 Garching, Germany, [‡]Department Chemie, Ludwig-Maximilians-Universität München, Butenandtstraße 5-13, D-81377 Munich, Germany, [§]SPECS GmbH, Voltastraße 5, D-13355 Berlin, Germany, and [⊥]Center for NanoScience (CeNS), Schellingstraße 4, D-80799 Munich, Germany

ABSTRACT The ordering transition of an amorphous carbon layer into graphene was investigated by high-temperature scanning tunneling microscopy. A disordered C layer was prepared on a Ru(0001) surface by chemical vapor deposition of ethylene molecules at ~660 K. The carbon layer grows in the form of dendritic islands that have almost the same density as graphene. Upon annealing of the fully covered surface, residual hydrogen desorbs and a coherent but still disordered carbon layer forms, with almost the same carbon coverage as in graphene. The ordering of this layer into graphene at 920 to 950 K was monitored as a function of time. A unique mechanism was observed that involves small topographic holes in the carbon layer. The holes are mobile, and on the trajectories of the holes the disordered carbon layer is transformed into graphene. The transport of C atoms across the holes or along the hole edges provides a low-energy pathway for the ordering transition. This mechanism is prohibited in a dense graphene layer, which offers an explanation for the difficulty of removing defects from graphene synthesized by chemical methods.

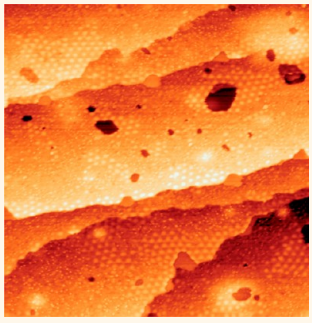

KEYWORDS: high-temperature STM · graphene · disorder−order transition · ethylene · Ru(0001) · TPD · CVD

Any future technology to synthesize graphene by epitaxial growth on metals will have to solve the problem of achieving low defect concentrations; in particular it has to keep boundaries between rotational domains at a minimum. One possible solution to this problem is to try to grow only one large single crystal of graphene covering an entire wafer. This approach has been greatly advanced by recent experiments with polycrystalline Cu foils on which graphene crystals of millimeter diameters were grown. After transfer, these samples showed charge carrier mobilities comparable to mechanically exfoliated graphene.[1,2] Of course, an applied process has to fulfill many further requirements, and it is currently not clear which substrate metal will give the best results. Metals that interact more strongly with graphene than Cu can direct the orientations of the graphene domains, offering a second possibility for growing high-quality graphene. Given a single-crystalline support of such a metal, graphene islands may coalesce without forming dislocations between rotational domains. With this approach millimeter-sized graphene domains were grown on Ir(111) by applying sequences of low-temperature chemical vapor deposition (CVD) and annealing.[3] This second method will usually not give perfect single crystals, so that the healing of defects, a fundamental question for any graphene synthesis method, plays a particularly important role here. The question is thus how defects can heal in a closed graphene layer on a metal surface. In contrast to the growth of epitaxial graphene from a 2D gas phase of adsorbed C atoms, which is pretty well understood, and to the annealing of relatively dilute C layers to form

* Address correspondence to wintterlin@cup.uni-muenchen.de.

Received for review August 1, 2012 and accepted December 7, 2012.

Published online December 07, 2012
10.1021/nn303468j

islands of graphene,[3−5] very little is known about the atomic processes when a more or less closed adsorbed graphene layer orders. One scanning tunneling microscopy (STM) investigation was focused on the ordering of a closed graphene layer on Ni(111),[6] but the data were taken *ex situ*, after cooling from the annealing temperature. There are also several simulations that indicate that the metal support plays an important role in the ordering process.[7−9]

Here we present a high-temperature STM investigation of the ordering of a monolayer of amorphous carbon into graphene. The STM, a SPECS STM 150 Aarhus HT, can be operated at temperatures of up to ~1300 K,[10] so that the ordering could be monitored as a function of time, with atomic resolution and at the temperature at which it occurs. The system studied was carbon on a Ru(0001) single crystal, a model for the relatively strongly interacting metal/graphene systems [graphene interacts even more strongly with Ru(0001) than with Ir(111)[11]].

To start with a defined state for the ordering experiments, we first prepared and characterized a full layer of disordered carbon, with a density as close as possible to the density of graphene and preferentially without residual hydrogen from the CVD. This was achieved by additional temperature-programmed desorption (TPD) experiments. The preparation of the layer was built on existing knowledge about the decomposition of ethylene, the most frequently used precursor molecule, on Ru(0001).[12−17] From vibrational spectroscopy and TPD it was known that, at temperatures below 300 K, adsorbed ethylene molecules on the Ru surface mainly decompose into ethylidyne (CH_3-C_{ad}). Annealing the ethylidyne layer leads to hydrogen desorption and to the formation of CH fragments, which then further decompose to give a disordered carbon layer, a process completed at approximately 650 to 730 K. At 750 K X-ray photoelectron spectroscopy (XPS) already showed carbon with a C 1s energy in the range of epitaxial graphene,[13,18] but small energy shifts at higher temperatures indicated further changes in the local chemical environment.[13] STM data of a carbon layer obtained by methane decomposition on Ru(0001) at 800 K showed islands that did not yet display the characteristic moiré pattern of the graphene overlayer formed at 1300 K, although the phonon modes of graphene had already developed.[19] On Pt(111) STM data showed a similar sequence of structures, an ethylidyne layer, then CH clusters, at 700 to 770 K structureless islands and at 1000 K graphene.[4] A recent high-temperature STM study on Rh(111) also showed a layer of molecules, then clusters, at 808 K islands that only partially displayed the graphene structure and at 975 K the full graphene structure.[5] In the case of Rh the dissolution of carbon in the bulk at elevated temperatures and segregation from the bulk complicate the picture.

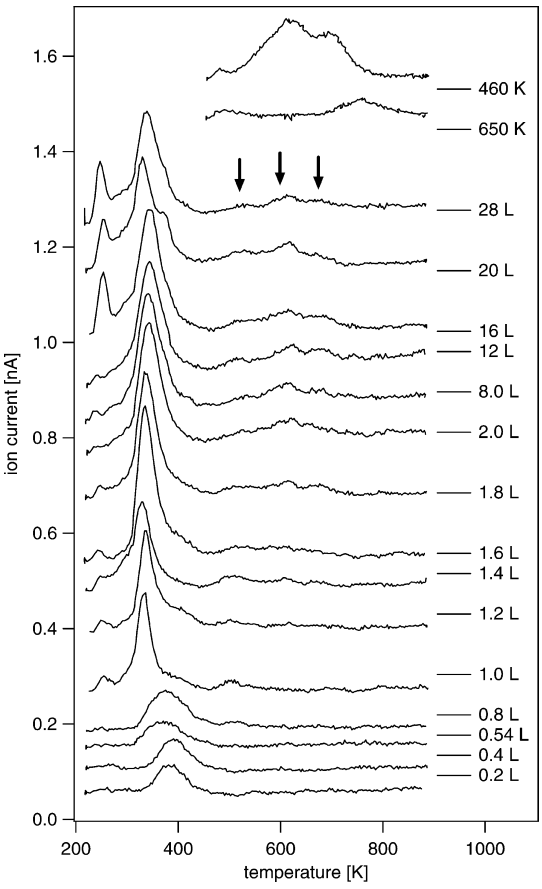

Figure 1. Hydrogen TPD spectra recorded after ethylene adsorption on Ru(0001) at 220 K. Ethylene exposures as indicated; heating rates 5 K s^{-1}. Arrows mark the three decomposition peaks at higher temperatures. The sharp peaks directly at the start of some of the spectra are artifacts from H_2 desorption from the heating filament. The top two TPDs were recorded after dosing 20 L of ethylene at 460 K (top) and 650 K (second from top). After the 650 K adsorption the sample was cooled to 460 K before the TPD.

These data suggest that on Ru(0001) between roughly 700 and 1000 K a disordered, partially already sp^2-hybridized network of C atoms orders to give graphene. How this ordering proceeds in a closed layer is unknown. In high-temperature STM experiments in this temperature window we found that the transition into graphene takes place by the motion of topographic holes in the graphene layer, a mechanism that has not been reported before for graphene. It explains the difficulties of removing defects from closed graphene layers, but also suggests possible solutions to this problem.

RESULTS

For reference purposes we first measured TPD data (Figure 1). Ethylene was adsorbed on the Ru surface at 220 K, and then the temperature was linearly ramped up with the sample in front of a small orifice in the housing of the quadrupole mass spectrometer (QMS) to record the desorption of hydrogen (see Methods). Before each TPD the sample was cleaned to remove the carbon layer formed in the previous run. The desorption spectra

show a large H_2 peak that shifts from 370 to 340 K with increasing ethylene dosage and then three less well-defined small peaks, at about 530, 610, and 680 K. This sequence of peaks and also the peak temperatures, within roughly ±20 K, are in good agreement with published TPD spectra.[12−15,17] The first peak is mainly attributed to the decomposition of ethylidyne to give CH and to the desorption of the initially split-off hydrogen from the metal surface. The following three peaks are interpreted as the stepwise decomposition of the CH layer.

The TPD spectra saturate at a dosage of approximately 2 langmuirs (L) of ethylene (1 L = 1.33 × 10^{-6} mbar s). Integration gives a H coverage of 0.57 monolayers (ML) at saturation (calibrated by means of H_2 adsorption on the Ru surface, which leads to a coverage of one ML of atomic hydrogen).[20] Since almost no ethylene desorbed in the TPDs, this corresponds to a C atom coverage of 0.28 ML that remains on the surface. With the known carbon coverage of 2.36 of the (25 × 25)-on-(23 × 23) graphene overlayer on Ru(0001)[21] the resulting surface fraction covered by graphene is only 0.28/2.36 = 0.12. Saturation of the Ru surface with ethylene at low temperature and annealing is thus not a suitable method for preparing a disordered carbon layer with the same density as graphene (in one step). At temperatures below 300 K, the space required by the fragments ethylidyne and hydrogen is too great [1/(0.14 ML) = 7 sites for each ethylidyne/hydrogen pair].

We therefore chose a higher adsorption temperature where the decomposition process is more complete, but, of course, staying below the temperature for graphene formation. A suitable temperature was expected to be indicated by a change in the sticking coefficient of the ethylene molecules. Measurements of the reactive sticking coefficient were performed at temperatures between 460 and 1020 K, following the method of Zhou *et al.*[22] The sample was placed closely in front of the orifice in the QMS housing, so that the gap between the sample surface and the housing was so small that line-of-sight molecular trajectories from the UHV chamber to the orifice were largely excluded. All molecules detected must therefore have been either reflected or desorbed from the sample surface.

To start an experiment, a constant ethylene pressure was adjusted. This caused a jump of the m/z = 26 QMS signal, which is specific for ethylene, to an initial value (Figure 2a, showing data for 660 K and p(ethylene) = 2.6 × 10^{-8} mbar). This initial m/z = 26 intensity is proportional to the fraction of ethylene molecules reflected from the clean Ru surface. The fraction is lower than unity because of the fraction of molecules decomposed on the surface. As a function of dosing time the fraction of reflected molecules increases because the empty surface area on which the ethylene molecules can decompose shrinks with the

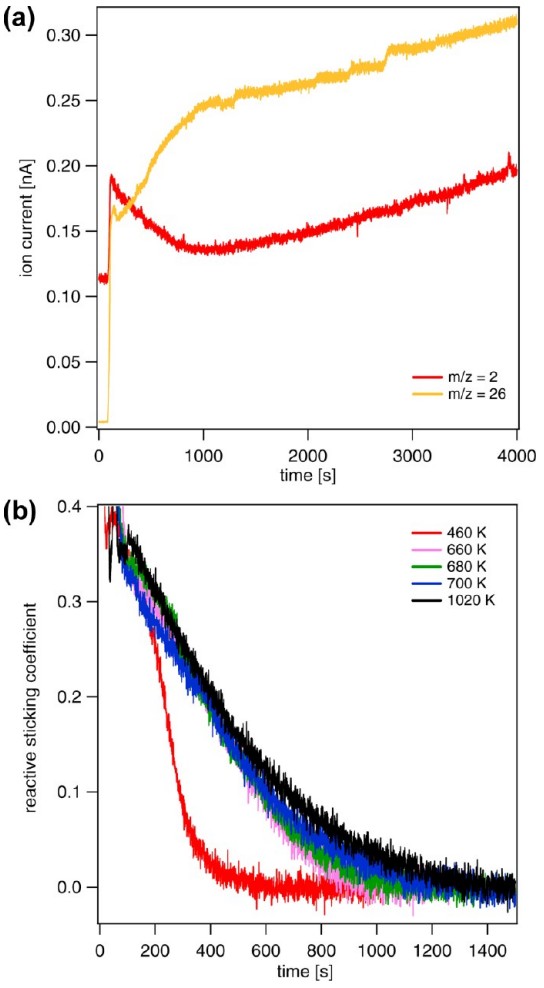

Figure 2. (a) QMS signal of ethylene (m/z = 26) and of hydrogen (m/z = 2) during ethylene dosing. (m/z = 26 is more specific for ethylene than m/z = 28 that is superimposed by CO.) T = 660 K, p(ethylene) = 2.6 × 10^{-8} mbar. (b) Reactive sticking coefficient of ethylene evaluated from corresponding data sets as in (a), for a series of temperatures.

formation of fragmentation products. After approximately 1000 s the signal levels off, indicating that the surface has become saturated by decomposition products. The following slow linear increase is caused by the limited pumping rate in the differentially pumped QMS unit and the continuous ethylene influx.

The m/z = 2 signal for hydrogen shows the opposite behavior (Figure 2a). The signal jumps to a high initial value and then decreases. The initial intensity is caused by hydrogen molecules formed by the reactive ethylene adsorption on the empty Ru surface. [At 660 K, which is close to the last hydrogen desorption peak (Figure 1), most of the hydrogen desorbs.] The signal then decreases because of the shrinking empty surface, until it also levels off at ∼1000 s. Figure 2a thus shows the consumption of ethylene and production of hydrogen by the CVD and the decreasing rate as the surface becomes covered by reaction products.

The reactive sticking coefficient $s(t)$ of the ethylene molecules was calculated from these data by first

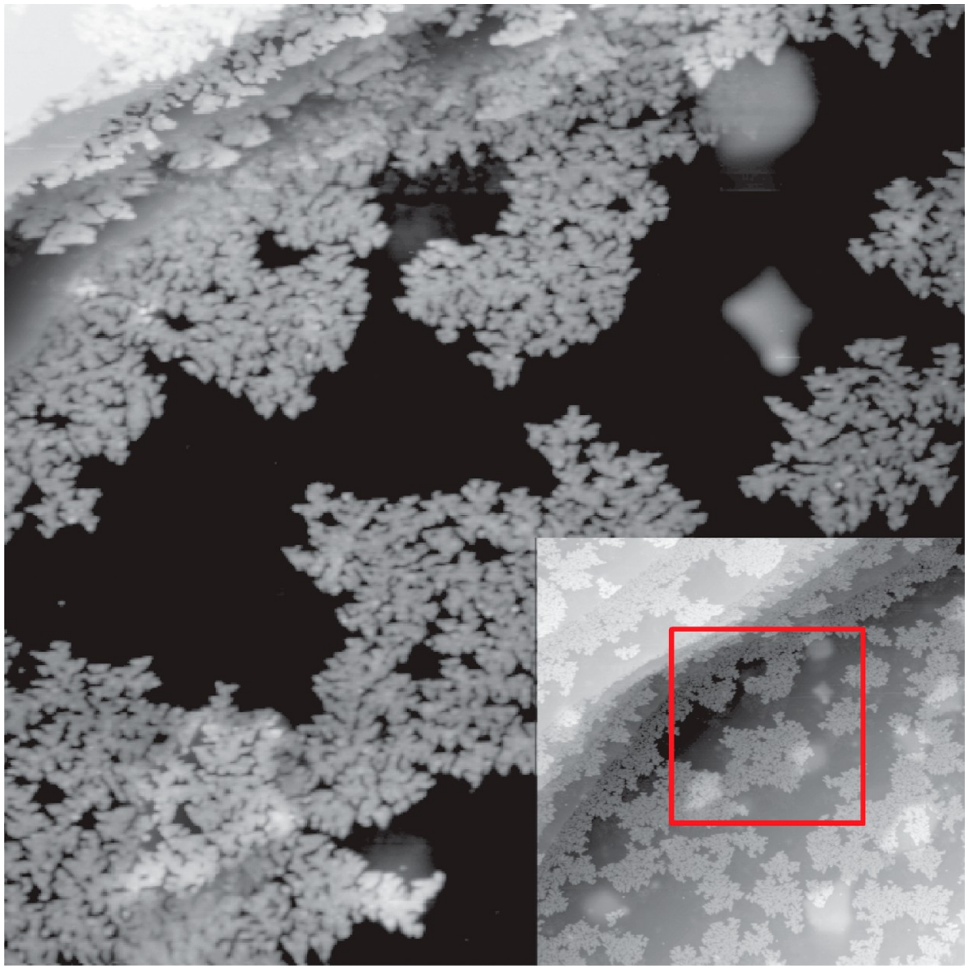

Figure 3. 1600 Å × 1600 Å STM image, recorded at a sample temperature of 660 K, after dosing of 12 L of ethylene at 660 K. The dendritic islands represent the carbon layer. The diffuse bright features are caused by residual Ar atoms in the Ru bulk resulting from sputter cleaning, a known effect for Ru.[25] The surface lattice is slightly deformed there, but this had no measurable effect on the graphene growth. Tunneling current 0.07 nA; tunneling voltage 1.24 V. Inset: 3200 Å × 3200 Å overview; the red box marks the area shown in the main figure.

correcting for the tilted baseline and then taking the difference of the $m/z = 26$ signal at saturation and at time instants t and dividing by the signal at saturation. Figure 2b shows the obtained $s(t)$ for several temperatures. The initial values are independent of temperature in the entire range between 460 and 1020 K ($s_0 = 0.4$). At 460 K the sticking coefficient first decreases linearly and then drops steeply, whereas for 660 K $\leq T \leq$ 1020 K the reactive sticking coefficients decrease almost linearly and at the same rates until saturation. A simple interpretation is that at 460 K, where the carbon layer still contains hydrogen (Figure 1, top trace), more or less isolated CH clusters are formed. If these are immobile, and as the ethylene molecules require several lattice sites to dissociate (~7 from the above estimate), the voids between the clusters at some point become too small for dissociation and the surface quickly saturates. This is in agreement with STM data from Pt(111), where the surface in this temperature range was covered by clusters, most likely consisting of CH.[4] The H_2 TPD, recorded after saturation at 460 K (Figure 1, top), confirms the presence of a significant amount of hydrogen (0.58 ML). At 1020 K, where well-ordered graphene is known to grow in the form of islands,[23] the $s(t)$ function decreases more or less linearly because the ethylene molecules decompose on the linearly decreasing empty surface with constant probability. At 660 to 700 K the $s(t)$ function shows almost the same behavior as at 1020 K, suggesting that also under these conditions carbon islands form, which are similarly dense as graphene. This interpretation is in agreement with the carbon coverages calculated by integrating the H_2 signals (from the intensity *vs t* data such as Figure 2a) and also by integrating the $s(t)$ curves obtained from the ethylene signal (Figure 2b). Both methods gave a carbon coverage of 2.0 ± 0.3 ML in the temperature range 660 to 700 K, corresponding to a fraction of 0.85 ± 0.13 of a graphene monolayer. On the other hand, the H_2 TPD, recorded after saturation at 650 K, still showed some H_2 desorption (0.06 ± 0.03 ML, Figure 1, second from top). The desorption peak at 760 K is at a significantly higher temperature than for the TPDs

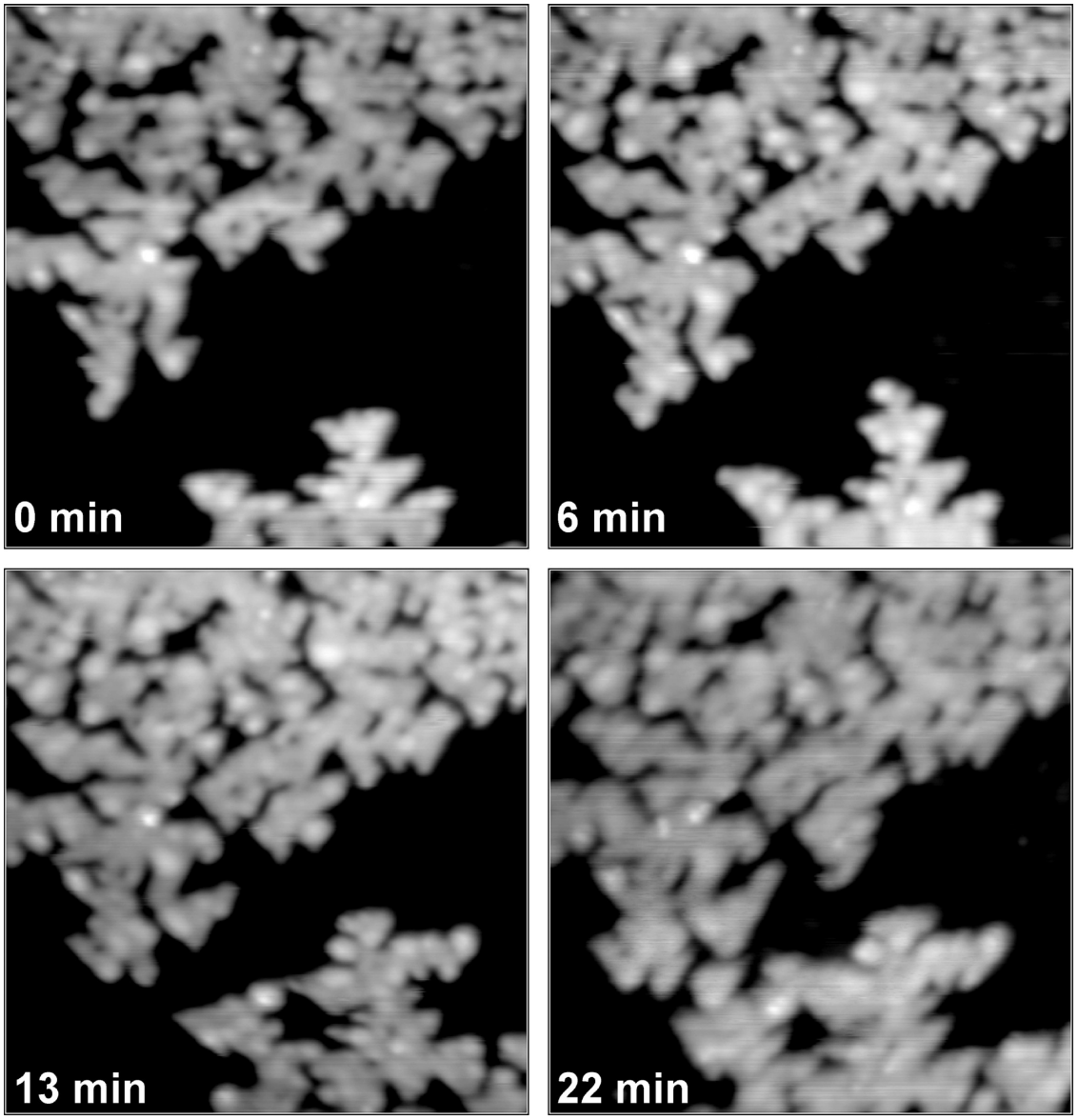

Figure 4. Series of STM images, taken during ethylene dosing at 660 K and *p*(ethylene) = 1.5 × 10^{-8} mbar. The dendritic carbon islands grow in units of triangular elements. 400 Å × 400 Å, tunneling current 0.07 nA, tunneling voltage 1.24 V. (Movie of full series available in the Supporting Information, movie 1.)

following dosing at 220 K. At 660 to 700 K ethylene adsorption thus leads to a full carbon layer with comparable density to graphene, the desired result. However, the layer contains a small amount of hydrogen.

We have started the STM experiments in this temperature range. Figure 3 shows an STM image recorded *in situ*, at 660 K, after ethylene dosing; the inset shows a larger overview of the area. The surface is partially covered by 2D dendritic islands, representing the carbon layer. The islands are homogeneously distributed on the extended terraces of the Ru surface and also decorate the ascending steps. The dendritic shape of the islands strongly differs from the compact islands typical for graphene.[11,24] The basic structure motif of the dendritic islands is an ill-defined triangle that itself consists of few round, connected features. All triangles on one terrace are equally oriented (one corner of all islands pointing downward on the central terrace in Figure 3) and rotated by 60° on the next terrace (one corner pointing upward). This alternating orientation must be caused by the A/B stacking of Ru, and it indicates a certain preferential orientation of the carbon overlayer with respect to the metal lattice.

On a smaller scale the growth of the dendritic islands at 660 K could be monitored in detail (Figure 4; a movie is available in the Supporting Information, movie 1). One can see that the growth is not continuous, but proceeds in steps that are more or less identical to the round features forming the triangles. Dendritic growth of an adsorbed layer is a typical observation for conditions determined by diffusion-limited aggregation. However, the finite width of the "arms" of the dendrites,

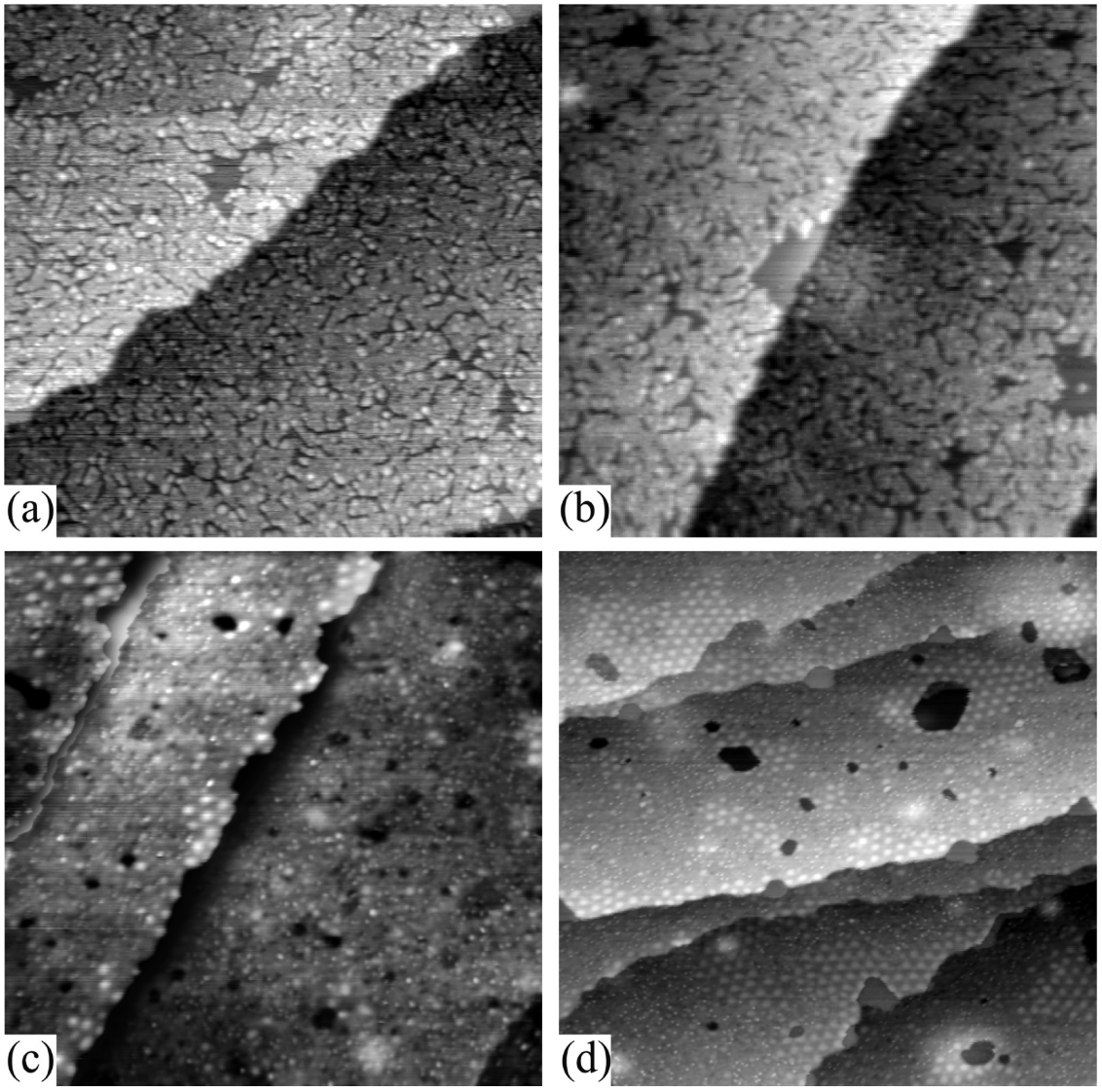

Figure 5. STM images recorded at increasingly higher temperatures after a saturation ethylene dose at 660 K (27 L); all images from different locations. (a) 660 K; the patterned structure results from the dendritic growth at this temperature; 800 Å × 800 Å. (b) 720 K; the patterned structure is still present; 800 Å × 800 Å. (c) 880 K; structure changes correlated with desorption of residual hydrogen and first moiré areas near step edges; 800 Å × 800 Å. (d) 950 K; the graphene moiré structure has appeared also on the terraces, but mostly near holes or at steps; 1120 Å × 1120 Å. Tunneling current 0.07 nA; tunneling voltage 1.24 V.

which are formed by the triangular structure elements, and the weak alignment of the triangles suggest that the diffusion-limited aggregation is combined with finite rearrangement processes within the structure units. An analogous model that combines diffusion-limited aggregation and edge diffusion at the perimeters of aggregates has been put forward to explain similar structures observed during metal-on-metal epitaxy.[26−28]

Structurally, the carbon film within the triangles, which have about 20 Å long sides, is relatively flat with some fine structure of round, brighter features. The characteristic moiré structure of the graphene overlayer on Ru(0001) has not yet formed. However, the carbon layer grown by CVD at 660 K has clearly started to form islands, in agreement with the sticking coefficient measurements. On a 20 Å length scale the film appears compact, whereas on a larger length scale it displays rifts resulting from the dendritic growth.

After saturation at 660 K the dendritic structure fills the entire surface (Figure 5a). On a small scale the structure displays the same flat areas and bright features; on a large scale it is characterized by the rifts. The hydrogen desorption signal from this surface [peak at 760 K, Figure 1, second from top TPD] is most likely related to these rifts. As suggested by the triangular symmetry of the building blocks of the dendrites, the compact parts represent a partially disordered, but locally already sp^2-hybridized carbon network. This would be consistent with the ~20 Å diameters of the triangular units, which is approximately the length scale on which the C atoms in a coherent sp^2 network form favorable bonds to the Ru atoms below.[29]

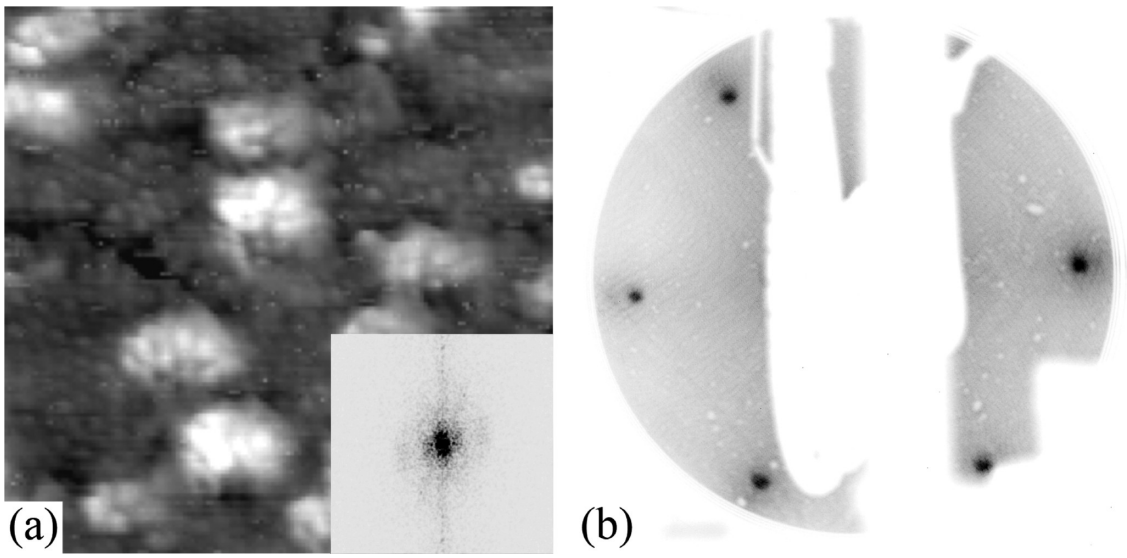

Figure 6. (a) Atomically resolved STM image and (b) LEED of the amorphous carbon-saturated layer obtained by ethylene dosing at 710 K. Tunneling conditions: 70 Å × 70 Å, 10 nA, −0.7 V, LEED energy 59 eV. Data taken after cooling to room temperature.

(An ordered graphene layer would form buckles on a 30 Å length scale because of the lattice mismatch with the Ru lattice.) The edges of such a network would exhibit sp^2-derived dangling bonds in the plane of the layer, and one can suppose that, at a growth temperature of 660 K, these are saturated by H atoms. If the network is mainly zigzag terminated and if all dangling bonds are occupied by H atoms, the length of the rifts, which was evaluated from the STM data, would correspond to a hydrogen coverage of 0.2 ML. From the TPDs after dosing in this temperature range a lower hydrogen coverage of 0.06 ± 0.03 ML was obtained, so that the edges can only be partially saturated. This makes sense because the carbon network can obviously grow under these conditions, and one expects that this requires free dangling bonds. The fact that the desorption temperature is 80 K higher than the last desorption peak in the usual TPDs, corresponding to an 11% (estimated 0.23 eV) higher desorption energy of these H atoms, is also not unreasonable. The energy to split off a hydrogen atom from benzene is 0.38 eV higher than from methane and also higher than from other aliphatic molecules.[30] If the CH layer formed during the usual TPDs (starting at 220 K, Figure 1) mainly consists of aliphatic carbon, whereas the layer formed at 660 K already contains sp^2 carbon, this would be consistent with the higher desorption temperature.

In a further set of experiments this state was cooled to room temperature and smaller scale STM images were recorded (Figure 6). [These experiments were performed with a thin, single-crystalline, (0001)-oriented Ru film supported on a Si(111) wafer on which graphene grows in the same way as on bulk Ru(0001). We have previously shown for Ir(111) that the bulk and the film system behave very similarly.[31]] The 70 Å × 70 Å STM image of a carbon film grown by CVD at 710 K (Figure 6a) shows atomic features with typical distances of 2.5 Å, corresponding to the unit cell of graphene. However, there is no apparent long-range order, and the Fourier transform of the image is featureless (inset of Figure 6a). The low-energy electron diffraction (LEED) pattern of this state (Figure 6b) shows the diffraction spots of the Ru substrate, whereas the typical satellites of the ordered graphene moiré structure are absent. It can be concluded that the sp^2 carbon layer obtained under these conditions is almost amorphous, except for a certain preferred rotational orientation, as suggested by the ill-defined triangles (Figures 3 and 4).

Starting with this layer the annealing experiments were performed [with the bulk Ru(0001) sample]. The temperature was raised in steps, and after each increase the temperature was kept constant to monitor the evolution of the film by STM (Figure 5). Between 660 K (Figure 5a) and 720 K (Figure 5b) no apparent changes are observed, and the carbon film displays the same rift structure. This is consistent with the fact that the temperature is still below the H_2 desorption peak at 760 K (Figure 1, second trace from top). At 880 K (Figure 5c), above the desorption peak, distinct changes are visible. Large parts of the film appear coherent, the rifts have mostly disappeared, but almost round holes have formed. Also at the steps voids have appeared. At some locations close to the atomic steps first small areas with a hexagonal structure (lattice constant approximately 30 Å) that characterizes the moiré structure of graphene are visible. These changes suggest that, after the hydrogen has fully desorbed, the rifts have closed. The moiré structure results from the lattice mismatch of the ordered graphene with the Ru(0001) substrate, so that we can use the moiré-covered surface fraction as an ordering parameter for the STM experiments. Most of the film is still flat and distinctly

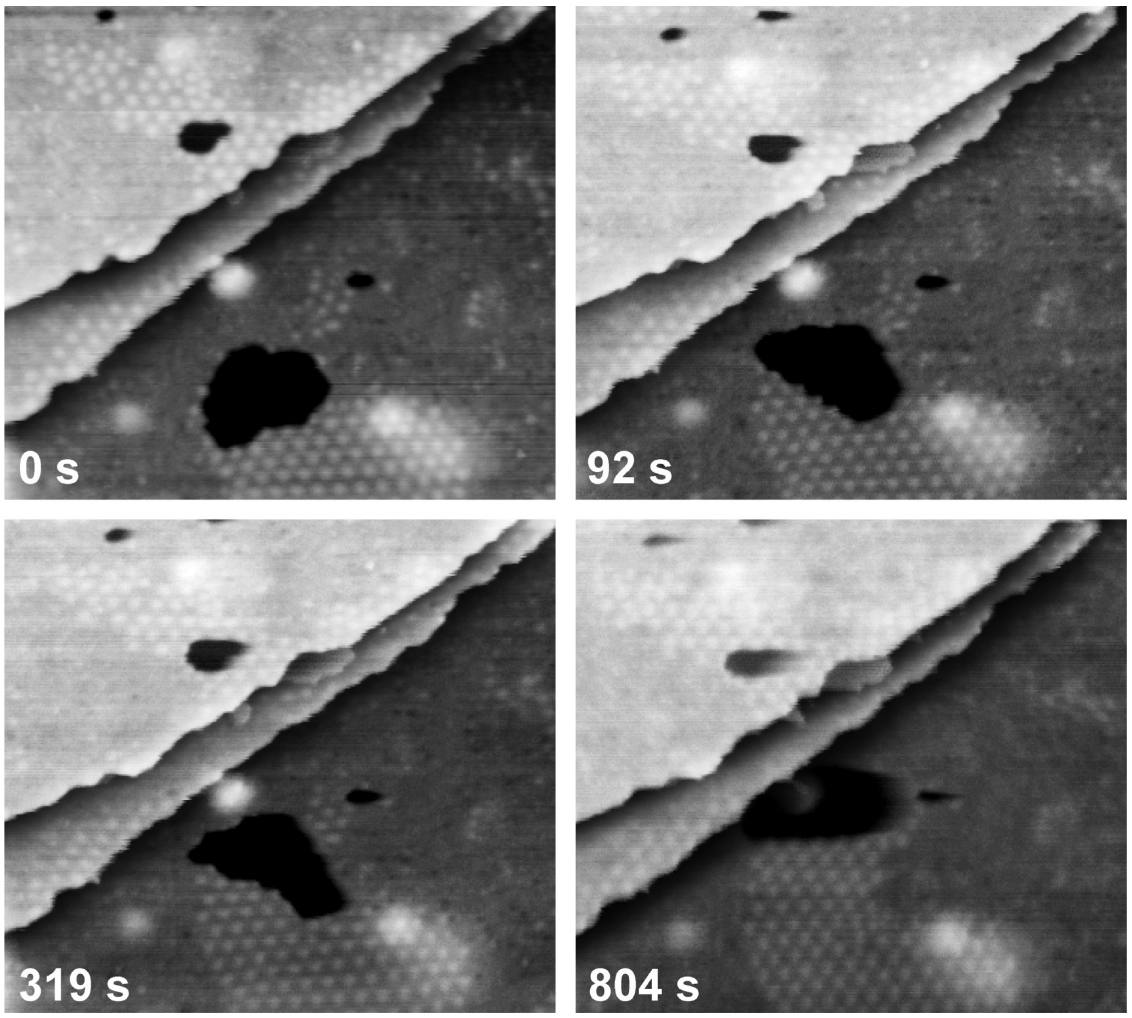

Figure 7. Series of STM images of the carbon-saturated layer, taken during the phase transition of the disordered carbon layer into graphene at 920 K. The motion of the hole on the central terrace transforms the flat, disordered carbon layer into the graphene moiré structure. 1100 Å × 1100 Å, tunneling current 0.07 nA, tunneling voltage 1.24 V. (Movie of full series available in the Supporting Information, movie 2.)

different from the moiré structure of graphene. However, the apparent height of the flat part of the layer is similar to that of the minima of the moiré phase, and the transitions to the moiré domains are smooth, supporting the interpretation as a disordered, but already sp^2-hybridized layer. The holes suggest that the average density in the initial structure was somewhat lower than a full ML, a result of the rifts. At 950 K (Figure 5d) there are fewer but larger holes, and larger domains showing the characteristic hexagonal pattern of the moiré structure have appeared. Most of the moiré-covered domains are located near one of the holes.

This spatial correlation between the holes and the moiré domains is no coincidence. Time sequences show that the holes are directly connected with the formation of the moiré structure. In the images of Figure 7, recorded at 920 K (a movie of the full series is available in the Supporting Information, movie 2), one can see that the holes are mobile. They travel through the carbon layer over unexpectedly large distances and in a seemingly directional, non-Brownian manner. Moreover, on the entire area across which the large hole in the image center of Figure 7 has moved the disordered carbon layer has transformed into the moiré structure of graphene. This was seen in several cases. Graphene is thus not formed homogeneously on the entire layer, but by a special growth process that involves the motion of topographic holes in the carbon layer. Most of the holes have two different sides, one bordered by disordered carbon, the other by graphene. Carbon atoms must be transported from the disordered sides of the holes to the graphene sides, causing the holes to move toward the disordered carbon and leaving behind graphene. The driving force for the directional motion of the holes is the different chemical potentials of carbon in the disordered form and in the graphene phase. Consistently with this explanation, holes completely surrounded by the moiré structure of the ordered graphene do not move. An example is the (larger) hole on the upper terrace in Figure 7.

It is clear that this mechanism can only work as long as the original disordered phase has a somewhat lower

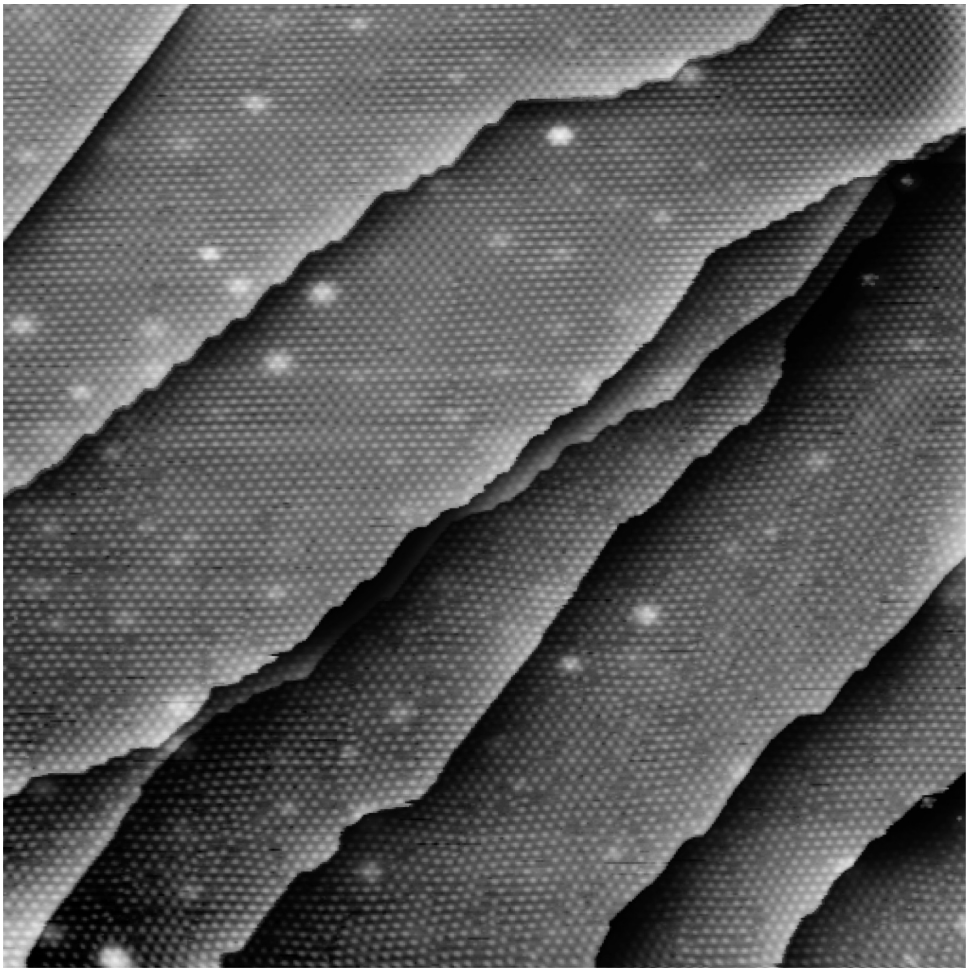

Figure 8. STM image after ethylene dosing at 940 K, recorded at room temperature. Initial *p*(ethylene) = 2 × 10^{-8} mbar; then the ethylene valve was closed. The gradient in the order from bottom to top is correlated with the decreasing growth rate. Total ethylene dosage 17.6 L, 2400 Å × 2400 Å, tunneling current 0.19 nA, tunneling voltage 1.4 V. (Larger image from another experiment available in the Supporting Information, movie 3.)

C coverage than the graphene; otherwise holes could not form. This may be one of the reasons for the difficulties of ordering once formed graphene. Figure 8 shows an STM image recorded after ethylene adsorption at 940 K. Data like these were typically obtained when the ethylene pressure was lowered during dosing. In this case the pressure was initially 2 × 10^{-8} mbar; then the valve was closed, but the decreasing ethylene pressure in the UHV chamber and the oversaturation coverage of adsorbed C atoms between the graphene areas were sufficient for the graphene to continue growing. The decreasing growth rate led to a dramatic improvement of the order during growth, here visible as persisting order gradient from the lower edge of the subsequently recorded image to the upper edge (Figure 8). In many cases the variation of the order could be spatially correlated with the time of the pressure reduction in the experiment (available as a "flyby" in the Supporting Information, movie 3). It should be noted that in these data the degree of order is higher than suggested by the disordered moiré areas because the visibility of the atomic disorder is strongly enhanced by the moiré effect.[32] Nevertheless, the data show that the disorder, formed at the higher pressure, is stable, despite the high temperature of 940 K, at which the dosing was performed. We suggest that this suppressed ordering is caused by the absence of holes in the fully developed graphene layer, so that atomic rearrangement processes are inhibited.

DISCUSSION

The STM data show that the disorder−order transition into graphene at 920 to 950 K does not occur homogeneously in the entire layer, but by a special mechanism involving small holes in the carbon film, which represent clusters of vacancies. At these holes C atoms from the edges are transported from disordered to ordered areas. Structure rearrangements in the interior of the amorphous layer are obviously connected with too high activation energies and do not lead to graphene at a measurable rate. This may be explained by the high connectivity within the disordered film, which most likely, at least partially, consists of sp^2-hybridized C. Such a structure is suggested by the STM images,

which show a dense layer, and also by the sticking coefficient measurements. The interpretation is in agreement with the C 1s binding energy of 285.0 eV, observed by XPS after annealing to 750 K,[13] which is already in the energy range of ordered graphene on Ru(0001) (where it varies between 284.52 and 285.12 eV because of the height modulation of the moiré structure).[18] It also agrees with the graphene phonon bands, observed by vibrational spectroscopy after methane CVD at 800 K.[19] That the film formed under such conditions does not yet display the moiré structure of graphene may be explained by its high defect concentration. The characteristic moiré structure of ordered graphene is connected with the horizontal stiffness of graphene, and this may be relaxed by defects.

For the transformation of this disordered film into graphene by the hole motion three different mechanisms appear possible. Carbon atoms may detach from the edges of the holes, move across the metal surface, and become attached at the opposite edges (possibly in the form of clusters). This leads to two limiting cases. In the first, the detachment of the C atoms from the disordered graphene edge is relatively fast (it does not cost so much energy to detach carbon from the disordered layer), and the attachment at the edge of the ordered moiré phase is rate limiting (activation energy 2.0 $\pm$ 0.1 eV[23]). In the second case the detachment from the disordered graphene edge is rate limiting, and the attachment at the ordered side is fast. In the first case a fast equilibrium is established between the disordered graphene edge and mobile C atoms in the vacancy hole. The concentration of the C atoms resulting from this equilibrium is higher than the C atom concentration in equilibrium with the ordered moiré structure (because of the lower stability of the disordered carbon), so that the C atoms in the vacancy holes are oversaturated (with respect to the ordered moiré structure). In the model of Loginova *et al.*[23] oversaturation of mobile C atoms determines the growth velocity of the graphene moiré structure. In the case considered here the growth velocitiy is identical to the hole velocity. Using the measured hole velocity (0.28 Å s^{-1} at 920 K from the data of Figure 7) and the analysis of Loginova *et al.* of the growth velocity, one can calculate the energy difference between the disordered and the ordered graphene structure. The obtained value, 0.05 eV per C atom, represents the driving force for the motion of the holes. The second case (detachment is rate limiting) is harder to analyze because an assumption about the preexponential factor of this complex process has to be made. Using $\nu_0 = 10^{13}$ s^{-1}, and the same activation energy as for the detachment from the ordered moiré structure (~2.3 eV[23]), the detachment rate leads to an order of magnitude higher hole velocity than the measured one. That the velocity is overestimated suggests that this mechanism is also feasible.

The third alternative is diffusion of C atoms or of groups of C atoms along the edges of the holes. Such processes have been investigated in simulations on free-standing graphene, and similar or somewhat higher activation energies than those considered above were found.[33] However, these simulations focused on the role of H atoms in these processes, and we can exclude the presence of H atoms at $T > 800$ K. In other simulations it was shown that the metal surface lowers the activation energy of ordering processes.[9] Transport along the edges can thus not be ruled out.

In any case, these low-energy transport processes are not possible for disordered layers without voids, and this provides an explanation for the difficulties of removing defects from extended graphene layers, even at higher temperatures. On the other hand, one could also make use of the hole mechanism for growing higher quality graphene on metal surfaces. Rather than trying to grow a full layer in one step, one could do the CVD in portions interrupted by annealing, so that the voids in the incomplete layers would help in the ordering process.

CONCLUSIONS

In conclusion, by using high-temperature STM, we have visualized the ordering of an amorphous carbon layer into graphene on a metal surface. The phase transition is mediated by holes in the carbon layer, which provide low-energy pathways for the transport of C atoms from disordered areas to graphene.

METHODS

The experiments were performed with three ultrahigh vacuum (UHV) chambers, one equipped with a high-temperature STM (SPECS STM 150 Aarhus HT), the second with a home-built beetle-type STM and Auger electron spectroscopy (AES), the third with another home-built STM, AES, and LEED. The high-temperature STM has already been successfully applied for graphene growth experiments at temperatures close to ~1300 K.[10] The instrument shows very low thermal drift. The second chamber was additionally equipped with a QMS mounted in a differentially pumped housing. For TPD measurements the sample was placed at a distance of 2 mm from a 3 mm hole in the housing, so that only molecules desorbing from the sample surface were detected.

The Ru(0001) sample was prepared according to an established procedure.[34] It consists of Ar^+ sputtering (6.5×10^{-5} mbar Ar, 1000 V, 20 min), annealing ($T > 1170$ K, 2 min), oxidation (2.6×10^{-7} mbar O_2, 920 K, 30 min), removal of oxygen by reduction (1.3×10^{-6} mbar H_2, 870 K, 30 min), and finally flash annealing (to >1270 K). For CVD the UHV chambers were backfilled with ethylene (Linde, purity 99.8%); pressures are uncorrected readings of the Varian ion gauge (which also enter the dosages given). However, to estimate the absolute C coverage from the $s(t)$ curves, the ion gauge reading was divided by 2.3, the gas correction factor for ethylene.

The data shown in Figure 6 are from a thin Ru(0001) film supported on a Si(111) wafer with a YSZ buffer layer. The preparation of the Ru film surface required only sputtering and

annealing. For the properties of such film systems with respect to graphene growth we refer to previous work on Ir(111).[31]

Conflict of Interest: The authors declare no competing financial interest.

Acknowledgment. This work was supported by the German Research Foundation (DFG) in the framework of the Priority Program 1459 "Graphene". We thank M. Schreck and M. Weinl, University of Augsburg, for providing the Ru film samples used for the experiment shown in Figure 6.

Supporting Information Available: Figures 4 and 7 are still images from longer time series. For a more intuitive illustration of the effects the full series were additionally compiled into movies. A further movie was compiled of data similar to Figure 8 that show an order gradient on a much larger length scale. This material is available free of charge *via* the Internet at http://pubs.acs.org.

REFERENCES AND NOTES

1. Petrone, N.; Dean, C. R.; Meric, I.; van der Zande, A. M.; Huang, P. Y.; Wang, L.; Muller, D.; Shepard, K. L.; Hone, J. Chemical Vapor Deposition-Derived Graphene with Electrical Performance of Exfoliated Graphene. *Nano Lett.* **2012**, *12*, 2751–2756.
2. Yan, Z.; Lin, J.; Peng, Z.; Sun, Z.; Zhu, Y.; Li, L.; Xiang, C.; Samuel, E. L.; Kittrell, C.; Tour, J. M. Toward the Synthesis of Wafer-Scale Single-Crystal Graphene on Copper Foils. *ACS Nano* **2012**, *10*, 9110–9117.
3. van Gastel, R.; N'Diaye, A. T.; Wall, D.; Coraux, J.; Busse, C.; Buckanie, N. M.; Meyer zu Heringdorf, F.-J.; Horn von Hoegen, M.; Michely, T.; Peolsema, B. Selecting a Single Orientation for Millimeter-Sized Graphene Sheets. *Appl. Phys. Lett.* **2009**, *95*, 121901.
4. Land, T. A.; Michely, T.; Behm, R. J.; Hemminger, J. C.; Comsa, G. Direct Observation of Surface Reactions by Scanning Tunneling Microscopy: Ethylene - Ethylidyne - Carbon Particles - Graphite on Pt(111). *J. Chem. Phys.* **1992**, *97*, 6774–6783.
5. Dong, G. C.; van Baarle, D. W.; Rost, M. J.; Frenken, J. W. M. Graphene Formation on Metal Surfaces Investigated by *In-Situ* Scanning Tunneling Microscopy. *New J. Phys.* **2012**, *14*, 053033.
6. Jacobson, P.; Stöger, B.; Garhofer, A.; Parkinson, G. S.; Schmid, M.; Caudillo, R.; Mittendorfer, F.; Redinger, J.; Diebold, U. Disorder and Defect Healing in Graphene on Ni(111). *J. Phys. Chem. Lett.* **2011**, *3*, 136–139.
7. Karoui, S.; Amara, H.; Bichara, C.; Ducastelle, F. Nickel-Assisted Healing of Defective Graphene. *ACS Nano* **2010**, *4*, 6114–6120.
8. Wang, Y.; Page, A. J.; Nishimoto, Y.; Qian, H.-J.; Morokuma, K.; Irle, S. Template Effect in the Competition between Haeckelite and Graphene Growth on Ni(111): Quantum Chemical Molecular Dynamics Simulations. *J. Am. Chem. Soc.* **2011**, *133*, 18837–18842.
9. Özçelik, V. O.; Cahangirov, S.; Ciraci, S. Epitaxial Growth Mechanisms of Graphene and Effects of Substrates. *Phys. Rev. B* **2012**, *85*, 235456.
10. Günther, S.; Dänhardt, S.; Wang, B.; Bocquet, M.-L.; Schmitt, S.; Wintterlin, J. Single Terrace Growth of Graphene on a Metal Surface. *Nano Lett.* **2011**, *11*, 1895–1900.
11. Wintterlin, J.; Bocquet, M.-L. Graphene on Metal Surfaces. *Surf. Sci.* **2009**, *603*, 1841–1852.
12. Barteau, M. A.; Broughton, J. Q.; Menzel, D. Vibrational Spectroscopy of Hydrocarbon Intermediates on Ru(0001). *Appl. Surf. Sci.* **1984**, *19*, 92–115.
13. Hrbek, J. Carbonaceous Overlayers on Ru(001). *J. Vac. Sci. Technol. A* **1986**, *4*, 86–89.
14. Hills, M. M.; Parmeter, J. E.; Mullins, C. B.; Weinberg, W. H. Interaction of Ethylene with the Ru(001) Surface. *J. Am. Chem. Soc.* **1986**, *108*, 3554–3562.
15. Henderson, M. A.; Mitchell, G. E.; White, J. M. The Coadsorption of Ethylene and CO on Ru(001). *Surf. Sci.* **1988**, *203*, 378–394.
16. Ransley, I. A.; Ilharco, L. M.; Bateman, J. E.; Sakakini, B. H.; Vickerman, J. C.; Chesters, M. A. Adsorption and Thermal Decomposition of Ethene and Propene on Ru(0001), Studied by *RAIRS*. *Surf. Sci.* **1993**, *298*, 187–194.
17. Livneh, T.; Asscher, M. The Adsorption and Decomposition of C_2H_4 on Ru(001): a Combined TPR and Work Function Change Study. *J. Phys. Chem. B* **2000**, *104*, 3355–3363.
18. Preobrajenski, A. B.; Ng, M. L.; Vinogradov, A. S.; Mårtenson, N. Controlling Graphene Corrugation on Lattice-Mismatched Substrates. *Phys. Rev. B* **2008**, *78*, 073401.
19. Wu, M.-C.; Xu, Q.; Goodman, D. W. Investigations of Graphite Overlayers Formed from Methane Decomposition on Ru(0001) and Ru(11−20) Catalysts with Scanning Tunneling Microscopy and High-Resolution Electron Energy Loss Spectroscopy. *J. Phys. Chem.* **1994**, *98*, 5104–5110.
20. Sun, Y.-K.; Weinberg, W. H. Determination of the Absolute Saturation Coverage of Hydrogen on Ru(001). *Surf. Sci.* **1989**, *214*, L246–252.
21. Martoccia, D.; Willmott, P. R.; Brugger, T.; Björck, M.; Günther, S.; Schlepütz, C. M.; Cervellino, A.; Pauli, S. A.; Patterson, B. D.; Marchini, S.; *et al.* Unit Cell of Graphene on Ru(0001): a 25×25 Supercell with 1250 Carbon Atoms. *Phys. Rev. Lett.* **2008**, *100*, 126102.
22. Zhou, L.; Günther, S.; Imbihl, R. Low-Pressure Methanol Oxidation over a Cu(110) Surface Under Stationary Conditions. *J. Catal.* **2005**, *230*, 166–172.
23. Loginova, E.; Bartelt, N. C.; Feibelman, P. J.; McCarty, K. F. Evidence for Graphene Growth by C Cluster Attachement. *New J. Phys.* **2008**, *10*, 093026.
24. Batzill, M. The Surface Science of Graphene: Metal Interfaces, CVD Synthesis, Nanoribbons, Chemical Modifications, and Defects. *Surf. Sci. Rep.* **2012**, *67*, 83–115.
25. Gsell, M.; Jakob, P.; Menzel, D. Effect of Substrate Strain on Adsorption. *Science* **1998**, *280*, 717.
26. Hwang, R. Q.; Schröder, J.; Günther, C.; Behm, R. J. Fractal Growth of Two-Dimensional Islands: Au on Ru(0001). *Phys. Rev. Lett.* **1991**, *67*, 3279–3282.
27. Röder, H.; Hahn, E.; Brune, H.; Bucher, J.-P.; Kern, K. Building One- and Two-Dimensional Nanostructures by Diffusion-Controlled Aggregation at Surfaces. *Nature* **1993**, *366*, 141–143.
28. Röder, H.; Bromann, K.; Brune, H.; Kern, K. Diffusion-Limited Aggregation with Active Edge Diffusion. *Phys. Rev. Lett.* **1995**, *74*, 3217–3220.
29. Wang, B.; Bocquet, M.-L.; Marchini, S.; Günther, S.; Wintterlin, J. Chemical Origin of a Graphene Moiré Overlayer on Ru(0001). *Phys. Chem. Chem. Phys.* **2008**, *10*, 3530.
30. Hioe, J.; Zipse, H. Radical Stability and its Role in Synthesis and Catalysis. *Org. Biomol. Chem.* **2010**, *8*, 3609–3617.
31. Zeller, P.; Dänhardt, S.; Gsell, S.; Schreck, M.; Wintterlin, J. Scalable Synthesis of Graphene on Single Crystal Ir(111) Films. *Surf. Sci.* **2012**, *606*, 1475–1480.
32. N'Diaye, A. T.; Coraux, J.; Plasa, T. N.; Busse, C.; Michely, T. Structure of Epitaxial Graphene on Ir(111). *New J. Phys.* **2008**, *10*, 043033.
33. Whitesides, R.; Frenklach, M. Detailed Kinetic Monte Carlo Simulations of Graphene-Edge Growth. *J. Phys. Chem. A* **2010**, *114*, 689–703.
34. Marchini, S.; Günther, S.; Wintterlin, J. Scanning Tunneling Microscopy of Graphene on Ru(0001). *Phys. Rev. B* **2007**, *76*, 075429.